

## Increased Confinement and $\beta$ by Inductive Poloidal Current Drive in the Reversed Field Pinch

J. S. Sarff, N. E. Lanier, S. C. Prager, and M. R. Stoneking

*University of Wisconsin, Madison, Wisconsin 53706*

(Received 8 October 1996)

With the addition of inductive poloidal current drive for current profile control in the Madison Symmetric Torus (MST) reversed field pinch, the magnetic fluctuation amplitude halves, leading to reduced energy and particle transport. A four- to five-fold increase in the energy confinement time to  $\tau_E \sim 5$  ms with both decreased Ohmic input power and increased stored thermal energy coincides with record low fluctuation amplitude and record high electron temperature  $\sim 600$  eV (for MST).  $\beta [= 2\mu_o\langle p\rangle/B(a)^2]$  increases from 6% to 8%. Other improvements include reduced electrostatic edge turbulence and plasma impurity content. [S0031-9007(96)02046-7]

PACS numbers: 52.55.Hc, 52.25.Fi, 52.25.Gj, 52.35.Py

A growing understanding of the turbulence in reversed field pinch (RFP) plasmas has inspired recent proposals to reduce magnetic fluctuations and associated transport by the application of current density profile control. The majority of the energy loss in an RFP plasma occurs through transport in a stochastic magnetic field generated by magnetic fluctuations. Most of these fluctuations result from several poloidal mode number  $m = 1$ , toroidal mode number  $n \sim 2R/a$ , magnetohydrodynamic (MHD) tearing instabilities [1] resonant in the core of the plasma and driven by the current density gradient. Direct measurements of the magnetic-fluctuation-induced particle [2] and heat [3] losses in the Madison Symmetric Torus (MST) identify large transport associated with these fluctuations. In other RFP experiments [4] the estimated magnetic-fluctuation-induced heat flux can account for the observed volume averaged heat flux. The fluxes measured in MST agree with expectations [5] for stochastic magnetic field diffusion, except the electron heat loss in the outer region of the plasma occurs at the ion rate [6]. Since tearing instability results from the current density gradient, the proposals for current profile control employ auxiliary electrostatic [7], rf [8,9], or neutral beam [10] current drive in the outer region of the plasma. In a conventional RFP plasma, the tearing fluctuations drive current in the outer region through a  $\langle \tilde{\mathbf{V}} \times \tilde{\mathbf{B}} \rangle$  motional emf or “dynamo” effect [11], establishing a self-consistent current profile. The auxiliary current drive, aimed to reduce the current density gradient, may be viewed as a replacement for dynamo current drive, reducing the fluctuations otherwise essential to sustain the RFP magnetic equilibrium.

In this Letter we describe the observation of reduced magnetic fluctuations and transport resulting from inductive poloidal current drive in an RFP. With poloidal current drive the magnetic fluctuation amplitude reaches a record low value for MST. The global energy confinement time increases four- to five-fold with both dramatically decreased Ohmic input power and increased stored thermal energy. A record high (for MST) electron temperature  $\sim 600$  eV is achieved, and the beta value in-

creases from 6% to 8%. In conventional RFP operation, an inductive toroidal electric field drives the plasma current. With the addition of a poloidal component, the electric field parallel to  $\mathbf{B}$  is increased in the outer region of the plasma (where the magnetic field is mostly poloidally directed) to facilitate current profile flattening for fluctuation suppression. Unlike the proposed electrostatic, rf, or neutral beam current drive, inductive poloidal current drive is inherently transient since it produces a changing toroidal flux in the plasma volume. The observed improvements last as long as poloidal current drive is present. We hereafter refer to this technique as pulsed poloidal current drive (PPCD).

The PPCD experiment is performed in MST [12], a large reversed field pinch with major radius  $R = 1.5$  m, minor radius  $a = 0.52$  m, toroidal plasma current  $I_\phi \leq 500$  kA, and beta  $\beta = 2\mu_o\langle p\rangle/B(a)^2 \leq 10\%$ . The wave forms of the toroidal and poloidal components of the electric field  $E_\phi = V_\phi/2\pi R$  and  $E_\theta = V_\theta/2\pi a$  (measured by loops at the plasma surface), the toroidal current  $I_\phi$ , the average toroidal magnetic field  $\langle B_\phi \rangle = \Phi/\pi a^2$ , and the toroidal field at the surface  $B_\phi(a)$  during a PPCD experiment are shown in Fig. 1. The shaded region indicates the time during which PPCD is applied. In the first PPCD experiment [13] the  $E_\theta$  drive was a single, triangular shaped pulse. Figure 1 illustrates improved PPCD that provides a series of four smaller pulses. Improved PPCD drives poloidal current more uniformly throughout the PPCD phase and reduces the plasma-wall interaction since the peak  $E_\theta$  amplitude of the four pulses is smaller. Also PPCD lasts longer, maintaining the beneficial effects observed in the first experiment for a longer period of time. Most importantly, improved PPCD leads to a greater reduction in the magnetic fluctuation amplitude and an increase of the stored thermal energy, energy confinement, and beta. The sharp negative spikes in  $E_\theta$  both before and after PPCD are associated with plasma-generated toroidal flux in spontaneous sawtooth (dynamo) events [Fig. 1(d)]. The negative  $E_\theta$  spikes represent the toroidal field magnet circuit’s inductive back

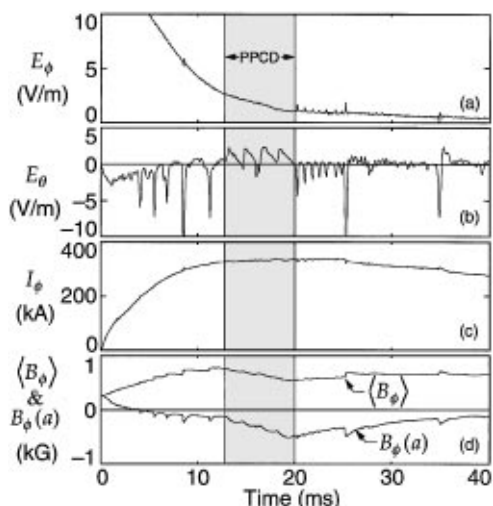


FIG. 1. Wave forms of the (a) surface toroidal electric field, (b) surface poloidal electric field, (c) toroidal plasma current, and (d) average and surface toroidal magnetic field.

reaction to dynamo flux generation within the plasma volume, and they oppose the dynamo-driven emf [14]. In contrast, PPCD is a controlled increase in the poloidal current through application of positive  $E_\theta$ .

A new result of improved PPCD is the reduction of the magnetic fluctuation amplitude to a record low value. The spatial root-mean-square magnetic field fluctuation  $\tilde{b}_{rms}$  measured in an improved PPCD discharge by a 32-station toroidal array of pickup coils on the plasma surface is shown in Fig. 2(a), normalized to the equilibrium field strength  $B(a)$ . The dominant wavelengths that compose this fluctuation are  $m = 1$ ,  $n = 6-10$  modes, although the  $m = 1$ ,  $n = 6$  mode alone accounts for most of the fluctuation during PPCD. Before PPCD is applied, the fluctuation amplitude cycles with the sawtooth oscillation at a cycle-averaged amplitude of  $\tilde{b}_{rms}/B(a) \approx 1.5\%$  typical of conventional RFP plasmas. PPCD suppresses sawtoothing, and the fluctuation amplitude first grows slowly and then decreases. Large sawteeth are suppressed in virtually all PPCD discharges, but the fluctuation amplitude in the first PPCD experiment [13] was held at the “between sawtooth crash” value. With improved PPCD the fluctuation in some discharges (like that of Fig. 2) is reduced *below* the sawtooth cycle minimum value to a record low value  $\tilde{b}_{rms}/B(a) \approx 0.8\%$ . During these periods of very low fluctuation the improvements in the plasma are most dramatic. The parallel electric field  $E_{||} = \mathbf{E} \cdot \mathbf{B}/B \approx E_\theta$  measured at the plasma surface is shown in Fig. 2(c) to emphasize the relationship of reduced magnetic fluctuation and poloidal current drive. While poloidal current is driven by PPCD, the fluctuation amplitude is small. Although large sawteeth are suppressed by PPCD, a new type of smaller sawtooth phenomenon [15] occurs during and immediately following improved PPCD. In Fig. 2(c) the presence of these smaller

sawteeth is evidenced through the negative  $E_{||}$  spike at  $t \approx 16$  ms during PPCD and by the series of negative spikes that immediately follow PPCD. The transition of the fluctuation to its low value coincides with a small sawtooth in this and many improved PPCD plasmas. This is probably related to an abrupt but modest current profile adjustment associated with the small sawtooth crash, but the current drive provided by an improved PPCD appears necessary as well. Periods of very low fluctuation are not observed when duplicating the original single pulse  $E_\theta$  programming. The details of the current penetration into the plasma (and therefore the current profile modification) depend on the time variation of the applied surface electric field. Improved PPCD resulted from ongoing attempts to optimize the inductive electric field programming.

In addition to the magnetic field, many quantities show reduced fluctuations during PPCD. For example, the voltage  $\varphi_{float}$  in Fig. 2(b) from a floating Langmuir probe located at the edge of the plasma shows a reduction in fluctuations similar to that in Fig. 2(a). [Note that Fig. 2(a) is a processed rms amplitude and Fig. 2(b) is a “raw” measurement.] Electrostatic fluctuations have been identified as the most likely cause of particle transport in the edge of MST [16] and other RFP experiments. A possible connection between the reduction of magnetic fluctuations in the core and electrostatic fluctuations in the edge is an exciting prospect. Current profile control may have a more general consequence than the targeted reduction of global magnetic fluctuations.

The global energy confinement time  $\tau_E$  increases up to five-fold during PPCD with both increased stored thermal energy and decreased Ohmic input power  $P_{Ohmic}$ . The shot-averaged [17] line density  $\bar{n}_e$ , central electron pressure  $n_{e0}kT_{e0}$ ,  $P_{Ohmic}$ , mean-squared magnetic fluctuation  $\tilde{b}^2$ , and  $H_\alpha$  radiation for 100 PPCD plasmas with

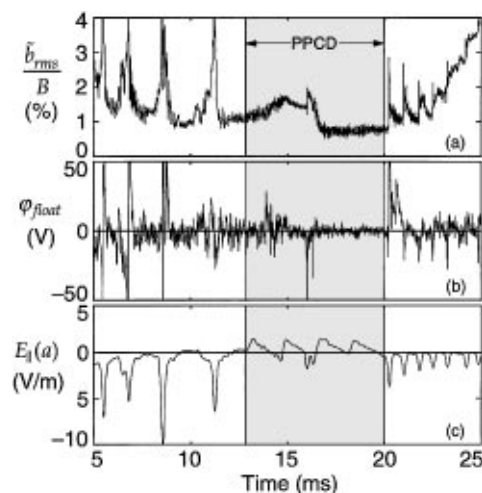


FIG. 2. The (a) spatial root-mean-square magnetic fluctuation, (b) edge floating Langmuir probe voltage, and (c) parallel electric field measured at the plasma surface during improved PPCD.

$I_\phi = 340$  kA are shown in Fig. 3. The shot averages of the same quantities for 60 conventional RFP plasmas are overlaid for comparison. For purposes of comparison, the gas fueling was adjusted for matched density evolution. The central electron pressure is measured with a single point (time and space) Thomson scattering diagnostic, varied in time shot by shot. In estimating  $\tau_E$  and  $\beta$ , the  $n(T_e + T_i)$  radial profile is assumed to behave as  $1 - (r/a)^2$ . (An 11-chord interferometer indicates the density profile is centrally peaked, but the temperature profiles are not measured.) The ion temperature measured by charge exchange is  $T_i^{cx} \approx 0.5T_{eo}$  in conventional discharges at this density but remains roughly constant while  $T_{eo}$  increases by as much as 70% compared with conventional RFP plasmas. The Ohmic input power is derived from the measured total input power (Poynting flux) at the plasma surface by subtracting the rate of change of stored magnetic energy using equilibrium modeling (described in the next paragraph). The calculation includes input power from both  $E_\phi$  and  $E_\theta$ . The PPCD plasmas in this ensemble, chosen only for the same density, have increased  $\tau_E$  from 1 to  $\sim 4$  ms and increased  $\beta$  from 6% to  $\sim 7\%$  compared with conventional RFP plasmas at a time near the end of PPCD ( $t \approx 17$  ms). [The poloidal beta  $\beta_\theta = 2\mu_o \langle p \rangle / B_\theta(a)^2$  increases from 6% to  $\sim 8\%$ .] A smaller ensemble of 25 plasmas which exhibit the exceptionally low magnetic fluctuation level features illustrated in Fig. 2(a) have  $\tau_E \approx 5$  ms and  $\beta \approx 8\%$  ( $\beta_\theta \approx 9\%$ ). Table I summarizes improved PPCD confinement (coincident with the lowest magnetic fluctuation) in 340 kA plasmas. An MST record  $T_{eo} = 615$  eV was measured for similar improved

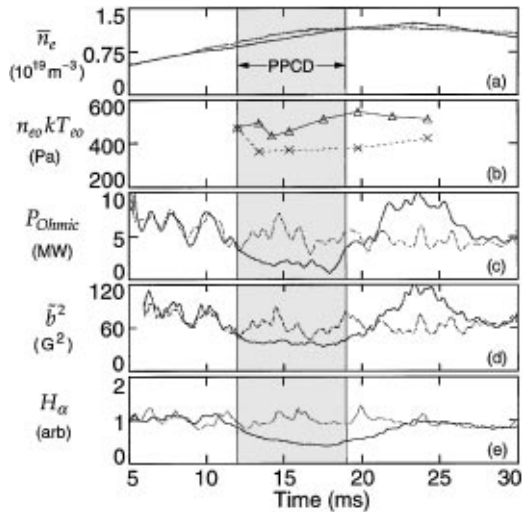


FIG. 3. Shot-averaged wave forms of (a) the central chord line density, (b) central electron pressure from Thomson scattering, (c) Ohmic input power, (d) mean-squared fluctuation amplitude, and (e)  $H_\alpha$  radiation. The unbroken lines are for PPCD plasmas, and the broken lines are for conventional RFP plasmas.

PPCD plasmas with higher current  $I_\phi = 440$  kA with  $\bar{n} \sim 1 \times 10^{19} \text{ m}^{-3}$ , although with smaller  $\beta \approx 7\%$  but similar  $\tau_E \approx 5$  ms.

Although the increase in stored thermal energy is substantial, most of the increase in  $\tau_E$  results from decreased transport, indicated by decreased  $P_{\text{Ohmic}}$ . Since PPCD is transient, accurate time-dependent equilibrium modeling is required to derive

$$P_{\text{Ohmic}} \equiv I_\phi V_\phi + I_\theta V_\theta - \frac{\partial}{\partial t} \int B^2 dV / 2\mu_o. \quad (1)$$

To evaluate the volume integrated (stored) magnetic energy in Eq. (1), the three-parameter cylindrical equilibrium model [18]

$$\nabla \times \mathbf{B} = \lambda_o(1 - r^\alpha)\mathbf{B} + (\beta_o/2B^2)\mathbf{B} \times \nabla p \quad (2)$$

is used to estimate  $\mathbf{B}(r, t)$  in lieu of direct magnetic profile measurements. The parallel-to- $\mathbf{B}$  current in Eq. (2) is specified by shape and amplitude parameters  $\alpha$  and  $\lambda_o$ , and the perpendicular current is specified by the central beta parameter  $\beta_o = 2\mu_o p_o / B_o^2$  and a pressure profile [assumed to be  $p(r) \propto 1 - r^2$ ]. The  $\alpha(t)$ ,  $\lambda_o(t)$ , and  $\beta_o(t)$  parameters are adjusted to match measured  $I_\phi(t)$ ,  $\langle B_\phi(t) \rangle$ ,  $B_\theta(a, t)$ , and  $\beta(t)$ . As a test of the model accuracy, the predicted “internal inductance”  $l_i \equiv 2 \int B_\theta^2 r dr / a^2 B_\theta(a)^2$  is compared with the internal inductance derived from the poloidal asymmetry in  $B_\theta$  at the plasma surface  $B_\theta(\theta) \approx \bar{B}_\theta(a) [1 + \frac{a}{R} \Lambda \cos \theta]$  measured by a 16-station poloidal array of magnetic sensors. The “asymmetry factor”  $\Lambda$  is related to  $l_i$  and  $\beta_\theta$  by  $\Lambda = l_i/2 + \beta_\theta - 1$  for a circular cross-section plasma [19]. The comparison is shown in Fig. 4, where superscript “ $\alpha$ ” identifies equilibrium model results. The “total inductance”  $L_{\text{tot}}/\mu_o R$ , which includes the toroidal field contribution to the total magnetic energy, is also shown in Fig. 4 to illustrate that  $\sim 2/3$  of the magnetic energy in an RFP is in the poloidal component (measured by  $l_i$ ). The good agreement between  $l_i$  determined from  $\Lambda$  and  $l_i$  predicted by Eq. (2) bolsters confidence in the calculation of  $P_{\text{Ohmic}}$ . The energy confinement time (quoted above) is defined as

$$\tau_E \equiv \frac{\int \frac{3}{2} nk(T_e + T_i) dV}{P_{\text{Ohmic}} - \frac{\partial}{\partial t} \int \frac{3}{2} nk(T_e + T_i) dV}. \quad (3)$$

TABLE I. MST confinement parameters with and without PPCD (compared at the same current and density near the end of the PPCD phase).

	PPCD	Conventional RFP
Current, $I_\phi$	340 kA	340 kA
Density, $n_e$	$1.0 \times 10^{19} \text{ m}^{-3}$	$1.0 \times 10^{19} \text{ m}^{-3}$
Temperature, $T_{eo}$	390 eV	230 eV
Poloidal beta, $\beta_\theta$	9%	6%
Input power, $P_{\text{Ohmic}}$	1.3 MW	4.4 MW
Fluctuation, $\tilde{b}_{\text{rms}}/B(a)$	0.8%	1.5%
Confinement, $\tau_E$	5 ms	1 ms

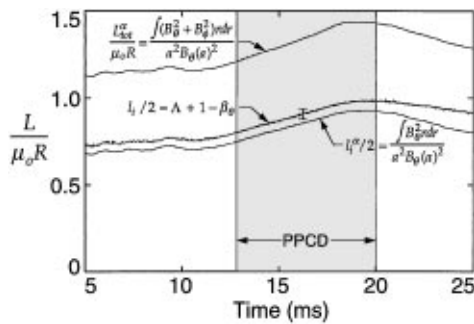


FIG. 4. Normalized inductances for ensemble data of Fig. 3. Superscript “ $\alpha$ ” indicates equilibrium model predictions [Eq. (2)]. For better illustration of the time evolution, this comparison is shown for fixed  $\beta_\theta = 10\%$ . [The temporal resolution of  $\beta(t)$  is coarse.]

Although thermal energy increasing during PPCD tends to decrease the denominator in Eq. (3), the impact of  $\partial\beta/\partial t > 0$  on the equilibrium modeling increases  $P_{\text{Ohmic}}$  by a slightly larger amount, and the net effect is a  $\leq 1$  ms decrease in  $\tau_E$  relative to a constant- $\beta$  calculation.

The global particle confinement time  $\tau_p$  also increases during PPCD. This is indicated by the decrease in  $H_\alpha$  emission (ionization source) while  $n_e$  increases. Particle transport modeling estimates  $\tau_p$  increases by a factor similar to the increase in  $\tau_E$ . Also the plasma is cleaner, as evidenced by reductions in the total radiated power, including visible impurity line radiation and bremsstrahlung radiation. Higher energy soft x-ray radiation increases, consistent with the higher electron temperature. Although clean wall conditions are necessary to avoid impurity contamination associated with pulsed  $E_\theta$ , improved PPCD does not require extreme conditioning measures. In the first PPCD experiment, boronization of the vacuum chamber was necessary to maintain impurity control.

In summary, inductive poloidal current drive decreases the amplitude of  $m = 1$  tearing fluctuations, suppresses their associated sawteeth, increases the plasma pressure, and increases the energy confinement time four- to five-fold in the MST RFP. The particle confinement time also increases. For the first time, the fluctuation amplitude falls below the “between sawtooth crash” level, and the confinement and beta improvements in the plasma are best during these periods of low magnetic fluctuation.

Although PPCD does not eliminate tearing fluctuations, a clear correlation exists between improved confinement, poloidal current drive, and fluctuation reduction. If the transported energy loss scales like  $\chi \propto \bar{B}_r^2$ , as expected for diffusion in a stochastic magnetic field [5], then the 50% reduction in the fluctuation amplitude predicts a four-fold decrease in energy transport. The observed four- to five-fold increase of the confinement time is consistent with this expectation.

The authors are grateful for the assistance of the MST group. This work was supported by the U.S. DOE.

- [1] D. D. Schnack, D. C. Barnes, Z. Mikic, D. S. Harned, and E. J. Caramana, *J. Comput. Phys.* **70**, 330 (1987); Y. L. Ho and G. G. Craddock, *Phys. Fluids B* **3**, 721 (1991), and references therein.
- [2] M. R. Stoneking *et al.*, *Phys. Rev. Lett.* **73**, 549 (1994).
- [3] G. Fiksel, S. C. Prager, W. Shen, and M. Stoneking, *Phys. Rev. Lett.* **72**, 1028 (1994).
- [4] For example, see I. H. Hutchinson *et al.*, *Nucl. Fusion* **24**, 59 (1984); K. Hattori *et al.*, *Phys. Fluids B* **3**, 3111 (1991).
- [5] J. D. Callen, *Phys. Rev. Lett.* **39**, 1540 (1977); A. B. Rechester and M. N. Rosenbluth, *Phys. Rev. Lett.* **40**, 38 (1978).
- [6] P. W. Terry *et al.*, *Phys. Plasmas* **3**, 1999 (1996).
- [7] Y. L. Ho, *Nucl. Fusion* **31**, 341 (1991).
- [8] E. Uchimoto *et al.*, *Phys. Plasmas* **1**, 3517 (1994).
- [9] S. Shiina, Y. Kondoh, and H. Ishii, *Nucl. Fusion* **34**, 1473 (1994).
- [10] K. Hattori, Y. Hirano, Y. Yagi, T. Shimada, and K. Hayase, *Fusion Technol.* **28**, 1619 (1995).
- [11] H. Ji *et al.*, *Phys. Plasmas* **3**, 1935 (1996).
- [12] R. N. Dexter, D. W. Kerst, T. H. Lovell, S. C. Prager, and J. C. Sprott, *Fusion Technol.* **19**, 131 (1991).
- [13] J. S. Sarff, S. A. Hokin, H. Ji, S. C. Prager, and C. R. Sovinec, *Phys. Rev. Lett.* **72**, 3670 (1994).
- [14] H. Ji, A. F. Almagri, S. C. Prager, and J. S. Sarff, *Phys. Rev. Lett.* **73**, 668 (1994).
- [15] J. S. Sarff *et al.*, *Phys. Plasmas* **2**, 2440 (1995).
- [16] T. D. Rempel *et al.*, *Phys. Rev. Lett.* **67**, 1438 (1991).
- [17] The PPCD programming for this ensemble is slightly different than for the single shot of Figs. 1 and 2.
- [18] V. Antoni *et al.*, *Nucl. Fusion* **26**, 1711 (1986).
- [19] J. P. Freidberg, *Rev. Mod. Phys.* **54**, 801 (1982).